

University of Dundee

Genetic recoding to dissect the roles of site-specific protein O-GlcNAcylation

Gorelik, Andrii; Galan Bartual, Sergio; Borodkin, Vladimir; Varghese, Joby; Ferenbach, Andrew; van Aalten, Daan

Published in:
Nature Structural & Molecular Biology

DOI:
[10.1038/s41594-019-0325-8](https://doi.org/10.1038/s41594-019-0325-8)

Publication date:
2019

Document Version
Peer reviewed version

[Link to publication in Discovery Research Portal](#)

Citation for published version (APA):

Gorelik, A., Galan Bartual, S., Borodkin, V., Varghese, J., Ferenbach, A., & van Aalten, D. (2019). Genetic recoding to dissect the roles of site-specific protein O-GlcNAcylation. *Nature Structural & Molecular Biology*, 26(11), 1071-1077. <https://doi.org/10.1038/s41594-019-0325-8>

General rights

Copyright and moral rights for the publications made accessible in Discovery Research Portal are retained by the authors and/or other copyright owners and it is a condition of accessing publications that users recognise and abide by the legal requirements associated with these rights.

- Users may download and print one copy of any publication from Discovery Research Portal for the purpose of private study or research.
- You may not further distribute the material or use it for any profit-making activity or commercial gain.
- You may freely distribute the URL identifying the publication in the public portal.

Take down policy

If you believe that this document breaches copyright please contact us providing details, and we will remove access to the work immediately and investigate your claim.

1 **Genetic recoding to dissect the roles of site-specific protein O-GlcNAcylation**

2 Andrii Gorelik¹, Sergio Galan Bartual¹, Vladimir S. Borodkin¹, Joby Varghese², Andrew T. Ferenbach¹
3 and Daan M. F. van Aalten^{1*}

4
5 ¹Centre for Gene Regulation and Expression and ²MRC Protein Phosphorylation and Ubiquitylation Unit,
6 School of Life Sciences, University of Dundee, Dundee, UK

7

8 *Correspondence to: dmfvanaalten@dundee.ac.uk

9 **Abstract**

10 Modification of specific Ser and Thr residues of nucleocytoplasmic proteins with O-GlcNAc, catalyzed by O-
11 GlcNAc transferase (OGT), is an abundant post-translational event essential for proper animal development
12 and dysregulated in various diseases. Due to the rapid concurrent removal by the single O-GlcNAcase
13 (OGA), precise functional dissection of site-specific O-GlcNAc modification *in vivo* is currently not possible
14 without affecting the entire O-GlcNAc proteome. Exploiting the fortuitous promiscuity of OGT, we show that
15 S-GlcNAc is a hydrolytically stable and accurate structural mimic of O-GlcNAc that can be encoded in
16 mammalian systems with CRISPR-Cas9 in an otherwise unperturbed O-GlcNAcome. Using this novel
17 approach, we target an elusive Ser405 O-GlcNAc site on OGA, showing that this site-specific modification
18 affects OGA stability.

19 Introduction

20 Protein O-GlcNAcylation is a ubiquitous and dynamic nucleocytoplasmic post-translational modification of
21 serines and threonines with O-linked β -*N*-acetylglucosamine (O-GlcNAc)¹. Thousands of protein substrates
22 are modified by O-GlcNAc transferase (OGT)² while a single enzyme, O-GlcNAc hydrolase (OGA)³,
23 removes the modification. Importantly, OGT is required for proper development in mice and fruit flies^{4,5}. On
24 the other hand, disruption of O-GlcNAc cycling on specific proteins is associated with cancer⁶, diabetes⁷,
25 neurodegeneration⁸ and a recently described intellectual disability syndrome⁹.

26 Functional dissection of individual O-GlcNAc sites has so far relied on alanine mutagenesis or modulation
27 of OGA or OGT activity through inhibition or knockdown. However, these approaches are confounded by
28 undesirable effects on the entire O-GlcNAcome. Methods for introducing site-specific stoichiometric O-
29 GlcNAc modification are limited to *in vitro* chemical biology techniques such as expressed protein ligation.
30 Yet, only a few O-GlcNAcylated proteins have been produced using this method, including tau and α -
31 synuclein^{10,11}. Another *in vitro* method, relying on the chemical conversion of a cysteine (introduced by site-
32 directed mutagenesis) to dehydroalanine and subsequent reaction with a GlcNAc derivative, is limited to
33 proteins that do not contain (many) native cysteine residues and is not stereo-specific¹². Site-specific
34 incorporation of O-GlcNAc in the context of a living biological system has not been achieved yet.

35 Given that the O-GlcNAc modification is prone to hydrolysis by OGA, site-specific O-GlcNAcylation in
36 cells, even if achieved, would not be permanent. Interestingly, OGA itself belongs to a plethora of OGT
37 substrates and the modification site (Ser405) is conserved among vertebrates (Fig. 1a)^{13,14}. Previously, this
38 O-GlcNAc modification was shown to be inducible by OGA inhibition, while being minimal at basal
39 conditions^{15,16}. However, studying this phenomenon presents a paradox – even if stoichiometric O-
40 GlcNAcylation of catalytically active OGA could be achieved, its own hydrolase activity would remove it.
41 Therefore, the investigation of the regulatory functions of O-GlcNAc modification on OGA, and other OGT
42 substrates, would require site-specific installation of an OGA-resistant functional mimic of O-GlcNAc.

43 A thio-linked GlcNAc (S-GlcNAc) has potential to resist OGA-mediated hydrolysis. It was initially shown
44 that the pseudo-substrate peptide Ala-Cys-(S-GlcNAc)-Ala inhibits a highly active bacterial OGA orthologue
45 from *Clostridium perfringens* (CpOGA) at low micromolar concentrations, implying that S-GlcNAc may be a
46 hydrolytically stable mimic of O-GlcNAc in the context of a peptide backbone¹⁷. The non-hydrolysable S-
47 GlcNAc modification has been successfully applied as an O-GlcNAcylation mimic *in vitro* in the context of
48 several recombinant proteins, such as casein kinase 2 (CK2), histone H2B, α -synuclein and tau¹⁸⁻²¹.

49 Therefore, S-GlcNAc, if site-specifically incorporated, presents an attractive candidate for studying the
50 effects of permanent O-GlcNAcylation. Nonetheless, production of such S-GlcNAcylated proteins has thus
51 far been limited to *in vitro* approaches. Here we establish a straightforward method for site-specific
52 installation of S-GlcNAc mimic *in vivo*, compatible with CRISPR-Cas9 genome editing. We show that the O-
53 GlcNAc site on the O-GlcNAcase regulates its half-life, adding to the growing body of evidence that
54 suggests a link between O-GlcNAcylation and protein stability.

55

56 Results

57 S-GlcNAc is a non-hydrolysable O-GlcNAc analogue

58 A prerequisite for the incorporation of S-GlcNAc as a stable O-GlcNAc mimic is resistance to the action of
59 OGA. Although some studies support this^{17,20}, we wondered whether S-GlcNAcylation would be resistant to
60 OGA hydrolysis in the context of human OGA (hOGA). To investigate this, short synthetic peptides (bearing
61 the S- or O-GlcNAc modification) derived from hOGA were subjected to treatment with CpOGA, a
62 promiscuous, bacterial orthologue of the human enzyme with elevated activity¹⁷. Analysis of the products by
63 MALDI-TOF mass spectrometry revealed loss of modification on the O-GlcNAcylated peptide after just 4 h
64 of CpOGA treatment (Fig. 1b), whereas the S-GlcNAcylated peptide remained intact for at least 24 h (Fig.
65 1b).

66 Next we asked whether the S-GlcNAc modification is an adequate structural mimic of the O-GlcNAc
67 modification in the context of proteins that recognize the O-GlcNAc modification, such as OGA and recently
68 discovered O-GlcNAc readers²². We employed a fluorescence polarimetry competition assay²³ to compare
69 the binding affinities of Ser-O-GlcNAc and Cys-S-GlcNAc in the context of a peptide, using a catalytically
70 incompetent mutant of CpOGA (CpOGA^{D298N}) as a model O-GlcNAc “reader”²⁴. Encouragingly,
71 CpOGA^{D298N} did bind the hOGA S-GlcNAcylated peptide with a K_D value in the μM range, albeit two orders
72 of magnitude lower than the O-GlcNAcylated equivalent (Fig. 1c). These data suggest that S-GlcNAc will
73 likely be recognized by a range of O-GlcNAc binding proteins, and is an adequate mimic of the O-GlcNAc
74 modification.

75 Although Cys-S-GlcNAc is expected to most accurately mimic Ser-O-GlcNAc, we wondered whether Thr-
76 O-GlcNAc could also be replaced with a non-hydrolysable S-GlcNAc. To investigate this, we synthesized O-
77 and S-GlcNAcylated peptides derived from the Thr72 O-GlcNAcylation site of α -synuclein¹¹ and subjected
78 them to treatment with active CpOGA. The latter completely removed the modification on Thr-O-GlcNAc

79 peptide after 24 h, while the Cys-S-GlcNAcylated counterpart remained stable (Extended Data Fig. 1a).
80 Interestingly in a binding assay, the affinity of inactive CpOGA for Cys-S-GlcNAcylated peptide was just one
81 order of magnitude weaker (Extended Data Fig. 1b). Thus, Cys-S-GlcNAc could potentially be used to
82 mimic Thr-O-GlcNAc.

83 To further corroborate the structural mimicry, we investigated whether the conformation of Cys-S-GlcNAc
84 is similar to Ser-O-GlcNAc in the context of a binding protein. We have previously reported crystal
85 structures of O-GlcNAcylated peptides in complex with CpOGA^{D298N}, including a complex with a peptide
86 encompassing Ser405 of hOGA²⁵. We soaked CpOGA^{D298N} crystals with the S-GlcNAcylated hOGA
87 peptide and obtained synchrotron diffraction data (Table 1). Molecular replacement with the previously
88 reported CpOGA structure revealed well-defined difference density covering the S-GlcNAc moiety and the
89 peptide backbone (Fig. 1d). Further refinement resulted in a final model with $R/R_{\text{free}} = 0.19/0.23$ (Table 1).
90 Comparison of the positions and conformations of the O- and S-GlcNAcylated peptides reveals them to
91 bind in a similar fashion (sugar atomic positional shifts $< 0.3 \text{ \AA}$, Fig. 1d) with conservation of the hydrogen
92 bonds of the sugar moiety with Asp401, Tyr335, Asn298 and Asp297 (Fig. 1d).

93

94 **S-GlcNAc can be genetically incorporated in the context of O-GlcNAc sites**

95 Having confirmed that S-GlcNAc appears to be a non-hydrolysable functional mimic of O-GlcNAc, we
96 sought a straightforward approach for site-specific incorporation of this modification *in vivo*. Interestingly,
97 the existence of S-GlcNAc on mammalian proteins was demonstrated recently²⁶. Moreover, using an *in vitro*
98 assay it was shown that cysteine residues in certain peptide sequences could be S-GlcNAcylated by
99 OGT²⁶. Inspired by this report, we hypothesized that OGT could modify cysteine residues in the context of
100 O-GlcNAcylation sites in proteins, such as a well-characterized single O-GlcNAcylation site (Ser395) on the
101 innate immunity signaling node TGF- β activated kinase binding protein 1 (TAB1)²⁷.

102 To test whether S395C mutation on TAB1 would result in S-GlcNAcylation, the recombinant protein was
103 incubated with OGT and UDP-GlcNAc followed by MS/MS analysis using Electron-Transfer/Higher-Energy
104 Collision Dissociation (ETHcD). In line with our hypothesis, cysteine-S-GlcNAcylation was unambiguously
105 detected on TAB1^{S395C} (Fig. 2a), confirming the reported S-GlcNAc transferase activity of OGT²⁶.

106 We have previously generated a site-specific O-GlcNAc TAB1 Ser395 antibody (gTAB1)²⁷ and used this
107 on Cys395 S-GlcNAcylated TAB1 to further investigate structural mimicry. In a control experiment, *in vitro*
108 OGT assay revealed a time-dependent increase of O-GlcNAcylation on wild type TAB1 using the gTAB1

109 antibody, while incubation with *Cp*OGA completely removed the modification (Fig. 2b). Likewise, a time-
110 dependent increase in TAB1^{S395C} GlcNAcylation was observed, indicating that S-GlcNAcylation represents
111 a suitable structural mimic recognizable by the gTAB1 antibody (Fig. 2b). Gratifyingly, TAB1^{S395C} S-
112 GlcNAcylation was resistant to *Cp*OGA treatment.

113 To investigate whether protein S-GlcNAc transferase activity of OGT could occur in a different substrate
114 sequence context, we generated a recombinant OGT linear fusion with a peptide derived from CK2 using a
115 previously described approach²⁸, in which the O-GlcNAcylation site was mutated to a Cys. In absence of a
116 site-specific antibody for CK2 O-GlcNAc site (Ser347), we used the pan-specific O-GlcNAc antibody
117 CTD110.6, which recognized both O-GlcNAcylation and S-GlcNAcylation CK2 fusion proteins (Extended
118 Data Fig. 2). The latter was resistant against *Cp*OGA hydrolysis, confirming our previous findings. Notably,
119 S-GlcNAcylation TAB1 was also detectable with CTD110.6 (Extended Data Fig. 3), suggesting that this
120 widely used antibody may be used as a tool to detect S-GlcNAcylation. These results are not entirely
121 surprising, since CTD110.6 can cross-react with *N*-glycans and GlcNAcylation O-mannose, as well as
122 terminal β -GlcNAc on complex *N*-glycans of cell surface glycoproteins²⁹⁻³¹. On the other hand, another pan-
123 specific O-GlcNAc antibody RL2 does not suffer from such poor specificity towards the linkage type³² and
124 reacted exclusively with O-GlcNAcylation TAB1 (Extended Data Fig. 3).

125 The crucial advantage of the OGT-assisted S-GlcNAcylation mimicry of protein O-GlcNAcylation is the
126 ability to encode it genetically in living systems by engineering targeted, single Ser or Thr to Cys mutations.
127 Having shown the application of our approach *in vitro*, we next investigated whether this could be extended
128 to cultured mammalian cells. FLAG-tagged wild type and Ser395Cys TAB1 were expressed in IL-1R
129 Hek293 cells²⁷ that were optionally treated with GlcNAcstatin G³³ to inhibit intracellular OGA. Additionally,
130 lysates were treated with *Cp*OGA to remove O-GlcNAc. As expected, O-GlcNAc-modified wild type TAB1
131 was detected, with the modification being sensitive to *Cp*OGA treatment (Fig. 2c). Strikingly, we also
132 detected GlcNAc modification on the Ser395Cys mutant, which was resistant to *Cp*OGA hydrolysis (Fig.
133 2c). In a separate experiment, treatment of cells overexpressing WT or S395C TAB1 with 4Ac5S-GlcNAc³⁴,
134 a metabolic precursor of the OGT inhibitor UDP-5S-GlcNAc, in both cases resulted in a disappearance of
135 signal detected by the gTAB1 antibody, suggesting that in cells the S-GlcNAc modification is enzymatic
136 (Extended Data Fig. 4).

137

138

139 **Genetically directed S-GlcNAcylation allows dissection of O-GlcNAc function on OGA**

140 Finally, we aimed to extend this approach to investigate the role of a single O-GlcNAc site on O-
141 GlcNAcase in cell culture. We pursued this goal by introducing the OGA Ser405Cys mutation in mouse
142 embryonic stem cells (mESCs) with CRISPR-Cas9. Potential knock-in mutants were screened and several
143 mutant lines were verified by sequencing (Supplementary Fig. 1-4). Due to the absence of a site-specific O-
144 GlcNAc OGA antibody as well as a lack of a proven immunoprecipitation-grade OGA antibody, we set out
145 to quantify the stoichiometry of the GlcNAc modification on OGA in cell lysates, by performing GalT^{Y289L}
146 labelling with GalNAz followed by click-chemistry reaction with an alkyne-labelled PEG 5000 to allow
147 separation of glycosylated and unmodified OGA by SDS-PAGE¹⁶. Although the galactosyltransferase
148 mutant GalT^{Y289L} is expected to label terminal GlcNAc residues, irrespective of the linkage type³⁵, this
149 approach has been mostly used for O-GlcNAc and terminal N-GlcNAc^{16,36}. To validate this method for S-
150 GlcNAc, we first performed OGT reactions with WT and S395C recombinant TAB1, followed by a reaction
151 with GalT^{Y289L} and subsequent PEGylation. Since the site-specific O-GlcNAc TAB1 antibody appears to
152 recognize both O- and S-GlcNAcylated TAB1 with similar sensitivity, we used it as a control to monitor the
153 successful OGT *in vitro* reaction as well as galactosyltransferase labelling efficiency based on the
154 disappearance of GlcNAc signal detected by a gTAB1 antibody (Extended Data Fig. 5). Western blot
155 analysis revealed complete labelling of S-GlcNAcylated TAB1, and comparable GlcNAcylation
156 stoichiometry, indicating similar efficiency of both O- and S-GlcNAc transferase activities of OGT (Extended
157 Data Fig. 5). Encouraged by these results, we applied this GlcNAc mass-tagging approach to OGA in
158 mESC lysates. Quantification of GlcNAcylation stoichiometry revealed a rather low O-GlcNAcylation of
159 OGA at a basal level (consistent with previously published data^{15,16}), while the S405C mutation resulted in a
160 GlcNAcylation stoichiometry of approximately 70%, similar to that induced by GlcNAcstatin G treatment on
161 the wild type protein (Fig. 3a). It must be noted that due to the enzymatic nature of GalT labelling, the
162 stoichiometry measured using this approach may be underestimated. Hyper-GlcNAcylation did not
163 significantly affect OGA and OGT levels, while the O-GlcNAcase activity was preserved (Fig. 3b and
164 Extended Data Fig. 6). Recent evidence has emerged suggesting that O-GlcNAcylation may directly affect
165 protein stability³⁷⁻³⁹. This prompted us to investigate whether modification of OGA with GlcNAc could have
166 an effect on its stability by monitoring the protein half-life (Fig. 3c). Interestingly, in a cycloheximide assay
167 hyper-GlcNAcylated OGA^{S405C} mutant had a significantly reduced half-life (approximately 6 h) compared to
168 wild type OGA (approximately 20 h). To investigate whether this was through a direct effect on OGA

169 stability, we performed a cell lysate thermal shift assay that revealed no significant differences between wild
170 type and S405C mutant OGA (Extended Data Fig. 7). Due to the fact that at basal conditions, OGA protein
171 level appears to be unchanged, we speculate that owing to a compensation mechanism to maintain O-
172 GlcNAc homeostasis, OGA^{S405C} may be synthesized at a faster rate to compensate for accelerated
173 degradation of a permanently S-GlcNAcylated protein. This suggests the presence of additional factors that
174 affect OGA stability in a GlcNAcylation dependent mechanism.

175

176 **Discussion**

177 In summary, we describe a simple and effective method for the rapid site-specific incorporation of a stable
178 O-GlcNAc analogue *in vitro* and in cells by harnessing the unexpected cysteine S-GlcNAc transferase
179 activity of OGT in combination with genome editing methods. We demonstrated that S-GlcNAc is a *bona*
180 *fide* O-GlcNAc mimic by determining the crystal structure of a synthetic S-GlcNAcylated hOGA-derived
181 peptide in complex with a model O-GlcNAc “reader” protein. We also showed that, despite micromolar
182 affinity, S-GlcNAcylation is stable against OGA hydrolysis in the context of the hOGA- and α -synuclein-
183 derived peptides. By mutating the corresponding O-GlcNAc site to a cysteine, we validated the OGT-
184 mediated S-GlcNAcylation approach on TAB1 and CK2 *in vitro* and for the former – in cells. Utilizing
185 CRISPR-Cas9 technology, we then directed OGT activity to the single specific site on OGA via genetic
186 encoding of a S405C mutation in mESCs and demonstrated quantitative S-GlcNAcylation of OGA, while
187 preserving its hydrolase activity. Intriguingly, this technique allowed us to provide the first insights into the
188 importance of O-GlcNAc removal from Ser405 of OGA for the maintenance of its stability, suggesting the
189 presence of a feedback regulation mechanism through as yet unknown additional factors. We anticipate
190 that site-specific incorporation of S-GlcNAc would be useful for studying O-GlcNAc modifications that
191 possess low stoichiometry due to the particularly rapid OGA-mediated hydrolysis. The S-GlcNAc genetic
192 recoding method is likely applicable to proteins with multiple O-GlcNAc sites. By sequential mutagenesis of
193 these sites to cysteines, it will be possible to dissect the roles of individual modifications. The added
194 advantage of this method *in vitro*, is the ability to remove the hydrolysis-prone O-GlcNAc modifications
195 through the action of OGA (*CpOGA*), leaving only S-GlcNAc modification on sites of interest intact. In
196 addition, we show that some of the detection tools available for O-GlcNAc modification (such as O-GlcNAc-
197 specific antibodies and galactosyltransferase labelling) can also be applied to S-GlcNAc. The key
198 advantage of our approach in cell studies is direct targeting of the residue of interest (a single atom

199 substitution in case of Ser to Cys mutation) without the need to express any artificial enzymatic machinery
200 or treat cells with chemical compounds. Cys mutagenesis can be easily performed by common molecular
201 biology techniques to study the modification *in vitro* and in an overexpression system. Moreover,
202 application of CRISPR-Cas9 gene editing technology now allows functional dissection of individual O-
203 GlcNAc sites on endogenous proteins in cells as well as model animals.

204

205 **Acknowledgements**

206 This work was funded by a Wellcome Trust Investigator Award (110061) to DvA and a Wellcome Trust 4-
207 year PhD studentship (105310/Z/14/Z) to AG. We thank Robert Gourlay and David Campbell (MRC PPU)
208 for assistance with mass spectrometry. We thank Olawale G. Raimi for purifying OGT-CK2 linear fusion
209 proteins. We would like to thank ESRF (beamline ID29) for the synchrotron time.

210

211 **Author contributions**

212 AG and DvA conceived the study; AG, SGB, VSB, JV, ATF performed experiments and analyzed data, AG
213 and DvA wrote the manuscript with input from all authors.

214

215 **Competing interests**

216 The University of Dundee holds a patent for the GlcNAcstatin inhibitor. The authors declare no other
217 competing interests.

218

- 220
- 221 1. Yang, X. & Qian, K. Protein O-GlcNAcylation: emerging mechanisms and functions. *Nat Rev Mol Cell Biol* **18**, 452–465 (2017). doi: 10.1038/nrm.2017.22
- 222
- 223 2. Haltiwanger, R. S., Holt, G. D. & Hart, G. W. Enzymatic addition of O-GlcNAc to nuclear and
- 224 cytoplasmic proteins: Identification of a uridine diphospho-N-acetylglucosamine: peptide beta-N-
- 225 acetylglucosaminyltransferase. *J. Biol. Chem.* (1990).
- 226 3. Gao, Y., Wells, L., Comer, F. I., Parker, G. J. & Hart, G. W. Dynamic O-glycosylation of nuclear and
- 227 cytosolic proteins: Cloning and characterization of a neutral, cytosolic beta-N-acetylglucosaminidase
- 228 from human brain. *J. Biol. Chem.* (2001). doi: 10.1074/jbc.M010420200
- 229 4. Shafi, R. *et al.* The O-GlcNAc transferase gene resides on the X chromosome and is essential for
- 230 embryonic stem cell viability and mouse ontogeny. *Proc Natl Acad Sci U S A* **97**, 5735–5739 (2000).
- 231 doi: 10.1073/pnas.100471497
- 232 5. Ingham, P. W. A gene that regulates the bithorax complex differentially in larval and adult cells of
- 233 *Drosophila*. *Cell* **37**, 815–823 (1984). doi: 10.1016/0092-8674(84)90416-1
- 234 6. Slawson, C. & Hart, G. W. O-GlcNAc signalling: implications for cancer cell biology. *Nat Rev*
- 235 *Cancer* **11**, 678–684 (2011). doi: 10.1038/nrc3114
- 236 7. Ma, J. & Hart, G. W. Protein O-GlcNAcylation in diabetes and diabetic complications. *Expert Rev*
- 237 *Proteomics* **10**, 365–380 (2013). doi: 10.1586/14789450.2013.820536
- 238 8. Yuzwa, S. A. & Vocadlo, D. J. O-GlcNAc and neurodegeneration: biochemical mechanisms and
- 239 potential roles in Alzheimer's disease and beyond. *Chem Soc Rev* **43**, 6839–6858 (2014). doi:
- 240 10.1039/c4cs00038b
- 241 9. Zachara, N. E. Critical observations that shaped our understanding of the function(s) of intracellular
- 242 glycosylation (O-GlcNAc). *FEBS Letters* (2018). doi: 10.1002/1873-3468.13286
- 243 10. Schwagerus, S., Reimann, O., Despres, C., Smet-Nocca, C. & Hackenberger, C. P. Semi-synthesis
- 244 of a tag-free O-GlcNAcylated tau protein by sequential chemoselective ligation. *J Pept Sci* **22**, 327–
- 245 333 (2016). doi: 10.1002/psc.2870
- 246 11. Marotta, N. P. *et al.* O-GlcNAc modification blocks the aggregation and toxicity of the protein alpha-
- 247 synuclein associated with Parkinson's disease. *Nat Chem* **7**, 913–920 (2015). doi:
- 248 10.1038/nchem.2361
- 249 12. Wright, T. H. *et al.* Posttranslational mutagenesis: A chemical strategy for exploring protein side-
- 250 chain diversity. *Science (80-.)*. (2016). doi: 10.1126/science.aag1465
- 251 13. Khidekel, N. *et al.* Probing the dynamics of O-GlcNAc glycosylation in the brain using quantitative
- 252 proteomics. *Nat Chem Biol* **3**, 339–348 (2007). doi: 10.1038/nchembio881
- 253 14. Whisenant, T. R. *et al.* Disrupting the enzyme complex regulating O-GlcNAcylation blocks signaling
- 254 and development. *Glycobiology* (2006). doi: 10.1093/glycob/cwj096
- 255 15. Teo, C. F. & Wells, L. Monitoring protein O-linked β -N-acetylglucosamine status via metabolic
- 256 labeling and copper-free click chemistry. *Anal. Biochem.* (2014). doi: 10.1016/j.ab.2014.06.010
- 257 16. Rexach, J. E. *et al.* Quantification of O-glycosylation stoichiometry and dynamics using resolvable
- 258 mass tags. *Nat. Chem. Biol.* (2010). doi: 10.1038/nchembio.412
- 259 17. Rao, F. V *et al.* Structural insights into the mechanism and inhibition of eukaryotic O-GlcNAc
- 260 hydrolysis. *EMBO J* **25**, 1569–1578 (2006). doi: 10.1038/sj.emboj.7601026
- 261 18. Tarrant, M. K. *et al.* Regulation of CK2 by phosphorylation and O-GlcNAcylation revealed by
- 262 semisynthesis. *Nat Chem Biol* **8**, 262–269 (2012). doi: 10.1038/nchembio.771
- 263 19. Raj, R., Lercher, L., Mohammed, S. & Davis, B. G. Synthetic Nucleosomes Reveal that
- 264 GlcNAcylation Modulates Direct Interaction with the FACT Complex. *Angew Chem Int Ed Engl* **55**,
- 265 8918–8922 (2016). doi: 10.1002/anie.201603106
- 266 20. De Leon, C. A., Levine, P. M., Craven, T. W. & Pratt, M. R. The Sulfur-Linked Analogue of O-GlcNAc
- 267 (S-GlcNAc) Is an Enzymatically Stable and Reasonable Structural Surrogate for O-GlcNAc at the
- 268 Peptide and Protein Levels. *Biochemistry* (2017). doi: 10.1021/acs.biochem.7b00268
- 269 21. Tegl, G. *et al.* Facile Formation of β -thioGlcNAc Linkages to Thiol-Containing Sugars, Peptides, and
- 270 Proteins using a Mutant GH20 Hexosaminidase. *Angew. Chemie - Int. Ed.* **58**, 1632–1637 (2019).
- 271 doi: 10.1002/anie.201809928
- 272 22. Toleman, C. A. *et al.* Structural basis of O-GlcNAc recognition by mammalian 14-3-3 proteins. *Proc.*
- 273 *Natl. Acad. Sci. U. S. A.* 201722437 (2018). doi: 10.1073/pnas.1722437115
- 274 23. Borodkin, V. S. *et al.* O-GlcNAcase Fragment Discovery with Fluorescence Polarimetry. *ACS Chem.*
- 275 *Biol.* (2018). doi: 10.1021/acschembio.8b00183
- 276 24. Selvan, N. *et al.* A mutant O-GlcNAcase enriches *Drosophila* developmental regulators. *Nat Chem*
- 277 *Biol* **13**, 882–887 (2017). doi: 10.1038/nchembio.2404

- 278 25. Schimpl, M., Borodkin, V. S., Gray, L. J. & van Aalten, D. M. Synergy of peptide and sugar in O-
279 GlcNAcase substrate recognition. *Chem Biol* **19**, 173–178 (2012). doi:
280 10.1016/j.chembiol.2012.01.011
- 281 26. Maynard, J. C., Burlingame, A. L. & Medzihradzsky, K. F. Cysteine S-linked N-acetylglucosamine (S-
282 GlcNAcylation), A New Post-translational Modification in Mammals. *Mol Cell Proteomics* **15**, 3405–
283 3411 (2016). doi: 10.1074/mcp.M116.061549
- 284 27. Pathak, S. *et al.* O-GlcNAcylation of TAB1 modulates TAK1-mediated cytokine release. *EMBO J* **31**,
285 1394–1404 (2012). doi: 10.1038/emboj.2012.8
- 286 28. Rafie, K. *et al.* Recognition of a glycosylation substrate by the O-GlcNAc transferase TPR repeats.
287 *Open Biol.* **7**, 170078 (2017). doi: 10.1098/rsob.170078
- 288 29. Ogawa, M. *et al.* GTDC2 modifies O-mannosylated α -dystroglycan in the endoplasmic reticulum to
289 generate N-acetyl glucosamine epitopes reactive with CTD110.6 antibody. *Biochem. Biophys. Res.*
290 *Commun.* **440**, 88–93 (2013). doi: 10.1016/j.bbrc.2013.09.022
- 291 30. Isono, T. O-GlcNAc-specific antibody CTD110.6 cross-reacts with N-GlcNAc₂-modified proteins
292 induced under glucose deprivation. *PLoS One* (2011). doi:10.1371/journal.pone.0018959
- 293 31. Tashima, Y. & Stanley, P. Antibodies that detect O-linked beta-D-N-acetylglucosamine on the
294 extracellular domain of cell surface glycoproteins. *J. Biol. Chem.* **289**, 11132–11142 (2014). doi:
295 10.1074/jbc.M113.492512
- 296 32. Reeves, R. A., Lee, A., Henry, R. & Zachara, N. E. Characterization of the specificity of O-GlcNAc
297 reactive antibodies under conditions of starvation and stress. *Anal. Biochem.* **457**, 8–18 (2014). doi:
298 10.1016/j.ab.2014.04.008
- 299 33. Dorfmüller, H. C. *et al.* Cell-penetrant, nanomolar O-GlcNAcase inhibitors selective against
300 lysosomal hexosaminidases. *Chem. Biol.* **17**, 1250–1255 (2010). doi:
301 10.1016/j.chembiol.2010.09.014
- 302 34. Gloster, T. M. *et al.* Hijacking a biosynthetic pathway yields a glycosyltransferase inhibitor within
303 cells. *Nat. Chem. Biol.* (2011). doi: 10.1038/nchembio.520
- 304 35. Ramakrishnan, B. & Qasba, P. K. Structure-based Design of β 1,4-Galactosyltransferase I (β 4Gal-
305 T1) with Equally Efficient N -Acetylgalactosaminyltransferase Activity . *J. Biol. Chem.* **277**, 20833–
306 20839 (2002). doi: 10.1074/jbc.M111183200
- 307 36. Boeggeman, E. *et al.* Direct identification of nonreducing GlcNAc residues on N-glycans of
308 glycoproteins using a novel chemoenzymatic method. *Bioconjug. Chem.* **18**, 806–814 (2007). doi:
309 10.1021/bc060341n
- 310 37. Gambetta, M. C. & Müller, J. O-GlcNAcylation Prevents Aggregation of the Polycomb Group
311 Repressor Polyhomeotic. *Dev. Cell* **31**, 629–639 (2014). doi: 10.1016/j.devcel.2014.10.020
- 312 38. Yuzwa, S. A. *et al.* Increasing O-GlcNAc slows neurodegeneration and stabilizes tau against
313 aggregation. *Nat Chem Biol* **8**, 393–399 (2012). doi: 10.1038/nchembio.797
- 314 39. Chu, C.-S. *et al.* O-GlcNAcylation regulates EZH2 protein stability and function. *Proc. Natl. Acad. Sci.*
315 **111**, 1355–1360 (2014). doi: 10.1073/pnas.1323226111
- 316
- 317

318 **Figure 1: S-GlcNAc mimics O-GlcNAc in the context of an OGA peptide**

319 **(a)** Schematic representation of the human OGA sequence (including the O-GlcNAcylation site
320 Ser405) and sequence conservation of Ser405 in vertebrates. GH domain – glycoside hydrolase
321 domain. HAT-like domain – histone acetyltransferase-like domain.

322 **(b)** MALDI-TOF mass spectra of synthetic O-/S-GlcNAc-modified peptides derived from hOGA with or
323 without CpOGA treatment for 4 and 24 h. Loss of GlcNAc residue is characterized by the reduction
324 in m/z by 203 Da. M – m/z, [M + Na] – m/z with a sodium adduct (23 Da), m/z – mass/charge ratio.

325 **(c)** Fluorescence polarization assay dose-response curves showing the displacement of a fixed
326 concentration of fluorescent probe (15 nM GlcNAcstatin B-FITC) from CpOGA^{D298N} by increasing
327 concentrations of O- or S-GlcNAcylated peptides derived from hOGA. Highest amount of probe
328 bound to CpOGA^{D298N} in the absence of competing O- or S-GlcNAcylated peptides was arbitrarily
329 set as 100%. Data points were fitted to a four-parameter equation for dose-dependent inhibition
330 using Prism (GraphPad). Data are shown as mean ± s.e.m. of n = 3 (O-GlcNAc peptide) and n = 4
331 (S-GlcNAc peptide) independent experiments. K_D values were calculated as described previously²³.

332 **(d)** Previously published O-GlcNAcylated hOGA-derived peptide (depicted as green sticks) in complex
333 with CpOGA^{D298N} (PDB: 2YDQ) and a crystal structure of S-GlcNAcylated hOGA-derived peptide
334 (purple sticks) in complex with CpOGA^{D298N} (deposited in the PDB as 6RHE). The unbiased $|F_o-F_c|$
335 map before inclusion of any S-GlcNAc peptide model is shown as a blue mesh contoured at 2.5σ .
336 CpOGA^{D298N} active site residues are shown as grey sticks. Hydrogen bonds are shown as dashed
337 lines.

338 Source data for panel c are available with the paper online.

339

340
341
342
343
344
345
346
347
348
349
350
351
352
353
354
355
356
357
358
359
360
361
362
363

Figure 2: OGT catalyzes S-GlcNAcylation of TAB1^{S395C} *in vitro* and in cells

- (a)** LC-MS/MS EthCD S-GlcNAc site mapping on S395C TAB1 mutant. *In vitro* S-GlcNAcylated S395C TAB1 mutant (7-409) was digested with trypsin and subjected to LC-MS. The tryptic peptide VYPVSVPYCSAQSTSK ($Mw_{calc} = 1918$ Da) containing a HexNAc (+203.1 Da) was detected. The observed fragment ions (z, y, c and b ion series) are indicated in the fragmentation diagram. Mass differences between y_7 to y_8 and c_8 to c_9 allow confirmation of C395 as the site of S-GlcNAc modification. The c_8^{2+} ion corresponds to m/z 461.75528.
- (b)** Time-course of TAB1^{WT} and TAB1^{S395C} *in vitro* OGT reaction. After 12 h incubation of TAB1^{WT} and TAB1^{S395C} with OGT, the reactions were treated with CpOGA. O- and S-GlcNAc modifications were detected by Western blot using an anti O-GlcNAc TAB1 (gTAB1) antibody.
- (c)** OGT catalyzes S-GlcNAcylation of TAB1^{S395C} in cells. IL-1R Hek293 cells were transfected with N-terminally FLAG-tagged TAB1 constructs that were wild type or carried S395C or S395A mutations of the O-GlcNAc modification site. The cells were treated with OGA inhibitor GlcNAcstatin G (GG) for to elevate O-GlcNAc levels. The lysate was then split in half and one half was treated with CpOGA to remove O-GlcNAc (as monitored by Western blot using an anti-O-GlcNAc antibody RL2). Overexpressed TAB1 levels were assessed with an anti-FLAG antibody. Glycosylation levels of TAB1 were monitored with a site-specific O-GlcNAc TAB1 antibody (gTAB1). Tubulin was used as a loading control. Normalization was performed by dividing the gTAB1 antibody signal (O-GlcNAc TAB1) by the FLAG signal (total TAB1). “*” denotes $P = 0.0377$, “****” denotes $P = 0.0001$, calculated by Student’s t -test (two-tailed, unpaired) Data are shown as mean \pm s.e.m. of $n = 3$ biological replicates. Uncropped Western blot images and source data for panel 2c are available with the paper online.

364 **Figure 3: OGT catalyzes hydrolytically stable cysteine-S-GlcNAcylation of OGA in cells, which**
365 **reduces OGA stability**

366 **(a)** Quantification of O- and S-GlcNAcylation stoichiometry on OGA was performed by chemoenzymatic
367 labelling with GalNAz using a galactosyltransferase Y289L mutant (GalT) and subsequent click-
368 chemistry reaction with a 5 kDa PEG-alkyne. Labelling was performed on cell lysates from cells
369 expressing wild type OGA (cells were either untreated or treated with 1 μ M GlcNAcstatin G (GG) as
370 a positive control) and OGA^{S405C} mutant. Reactions were assessed by Western blot using an anti-
371 OGA antibody. Upward molecular weight shift corresponds to GlcNAc modified OGA (gOGA).
372 Plotted are the GlcNAcylation stoichiometries of wild type (undetectable) and S405C mutant OGA.
373 Data are shown as mean \pm s.e.m. of n = 3 biological replicates.

374 **(b)** Quantification of OGA and total O-GlcNAc levels in wild type OGA and OGA^{S405C} mutant mES cells
375 by Western blot analysis. α -tubulin was used as a loading control. Data are shown as mean \pm s.e.m.
376 of n = 6 (WT OGA) and n = 9 (OGA^{S405C}) biological replicates. NS – no significant difference
377 (analyzed by two-tailed Student's *t*-test).

378 **(c)** OGA stability was measured by treating cells with cycloheximide at a final concentration of 20 μ g/ml
379 and harvesting cells at indicated time points for Western blot analysis using an anti-OGA antibody.
380 Normalization of band intensities was performed by dividing OGA signal by α -tubulin signal.
381 Untreated normalized sample was assigned as 100% OGA. “*” denotes $P = 0.0399$, “***” denotes $P =$
382 0.00115 , calculated by Student's *t*-test (two-tailed, unpaired). Data are shown as mean \pm s.e.m. of n
383 = 6 biological replicates (using three independent replicates for clones 27, 36 and two independent
384 replicates for clones 37, 39, 74). CHX – cycloheximide. Uncropped Western blot images and source
385 data for panels a-c are available with the paper online.

386

387 **Table 1. Data collection and refinement statistics.**

CpOGA–hOGA (S-GlcNAc) peptide 388 (PDB 6RHE)	
Data collection	
Space group	P6 ₁
Cell dimensions	
<i>a</i> , <i>b</i> , <i>c</i> (Å)	117.7, 117.7, 147.9
α , β , γ (°)	90°, 90°, 120°
Resolution (Å)	48.17 - 3.1 (3.21 - 3.1) ^a
<i>R</i> _{merge}	0.1077 (1.123)
<i>I</i> / σ <i>I</i>	9.13 (1.10)
<i>CC</i> _{1/2}	0.994 (0.379)
Completeness (%)	93.85 (95.67)
Redundancy	3.2 (3.3)
Refinement	
Resolution (Å)	48.17-3.1
No. reflections	19790 (1990)
<i>R</i> _{work} / <i>R</i> _{free}	0.1949/0.2270
No. atoms	
Protein	4594
S-GlcNAc peptide	43
Cadmium ion	25
Water	28
<i>B</i> -factors	
Protein	84.34
S-GlcNAc peptide	112.10
Cadmium	138.30
Water	69.83
R.m.s. deviations	
Bond lengths (Å)	0.013
Bond angles (°)	1.61

389 The dataset was collected from a single crystal. ^aValues in parentheses are for highest-resolution shell.

390 **Materials & Methods**

391

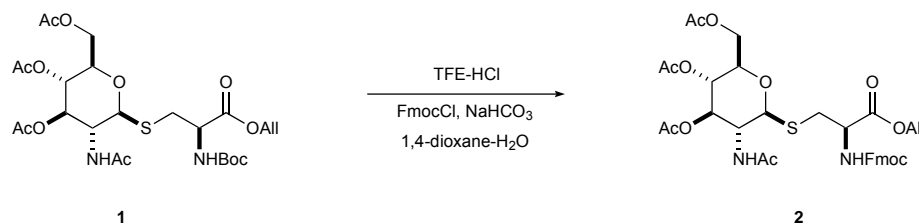
392 *Glycopeptide synthesis*

393 Peptides VAHS(**O-GlcNAc**)GA, VAHC(**S-GlcNAc**)GA, GAVVT(**O-GlcNAc**)GVTA and GAVVC(**S-**
394 **GlcNAc**)GVTA were synthesized as described previously²⁵, using 3,4,6-triacetyl-O-GlcNAc-Fmoc-Ser-OH
395 and 3,4,6-triacetyl-S-GlcNAc-Fmoc-Cys-OH as building blocks.

396

397 *Synthesis of Cys-S-GlcNAc building block*

398 Details of instrumentation and analytical procedures were reported elsewhere⁴⁰. Fmoc-GlcNAc-S-Cys-OAll
399 was prepared from Boc-GlcNAc-S-Cys-OAll⁴¹.

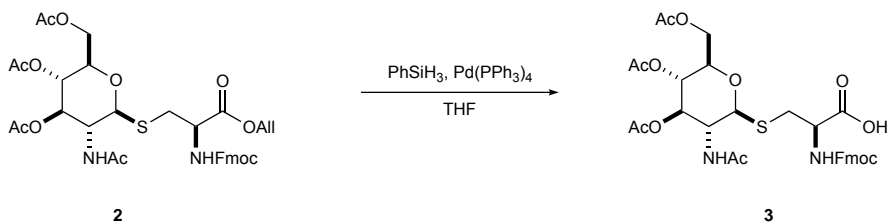


400

401 To a stirred solution of **1** (1.98 g, 3.35 mmol) in trifluoroethanol (TFE; 20 mL) concentrated HCl (1.5 mL)
402 was added at RT. The reaction mixture was further stirred for 45 min; *t*_{lc} [PE-DCM]-Me₂CO 30% showed
403 complete consumption of the starting material and formation of a more polar product. The reaction was
404 diluted with CHCl₃ and toluene, concentrated, and briefly dried in vacuum. The residue was dissolved in
405 1,4-dioxan-water 3:1 mixture (40 mL) and treated sequentially with solid NaHCO₃ (0.76 g, 9 mmol) and
406 FmocCl (1 g, 4 mmol). The clear solution with some solid deposit was stirred at RT for 1 h; *t*_{lc}
407 [PE-DCM]-Me₂CO 40% showed formation of a less polar new product. The residue was purified by flash-
408 column chromatography [PE-DCM 4:1]-Me₂CO 10→40% to give 2.35 g (3.33 mmol, quant) of the target
409 product as amorphous solid.

410 ¹H NMR (500 MHz, DMSO-*d*₆) δ 7.94 (d, *J* = 9.4 Hz, 1H), 7.90 (d, *J* = 7.6 Hz, 2H), 7.75 (d, *J* = 8.1 Hz, 1H),
411 7.72 (d, *J* = 7.5 Hz, 2H), 7.43 (t, *J* = 7.4 Hz, 2H), 7.37 – 7.31 (m, 2H), 5.91 (ddt, *J* = 17.2, 10.5, 5.2 Hz, 1H),
412 5.34 (dq, *J* = 17.3, 1.7 Hz, 1H), 5.21 (dq, *J* = 10.5, 1.6 Hz, 1H), 5.10 (t, *J* = 9.8 Hz, 1H), 4.88 (t, *J* = 9.7 Hz,
413 1H), 4.78 (d, *J* = 10.4 Hz, 1H), 4.61 (dt, *J* = 5.1, 1.6 Hz, 2H), 4.38 (td, *J* = 8.8, 4.9 Hz, 1H), 4.35 – 4.28 (m,
414 2H), 4.25 (t, *J* = 6.9 Hz, 1H), 4.14 (dd, *J* = 12.3, 5.1 Hz, 1H), 4.03 (dd, *J* = 12.2, 2.4 Hz, 1H), 3.92 (q, *J* =
415 10.3 Hz, 1H), 3.86 (ddd, *J* = 10.1, 5.0, 2.5 Hz, 1H), 3.15 (dd, *J* = 13.8, 4.8 Hz, 1H), 2.85 (dd, *J* = 13.8, 9.4

416 Hz, 1H), 1.99 (s, 3H), 1.99 (s, 3H), 1.93 (s, 3H), 1.76 (s, 3H) (Supplementary Fig. 5). m/z (ESI-TOF) found:
417 713.2344 expected for C₃₅H₄₀N₂O₁₂S (M+H⁺), 713.2380



418
419 To a cold (ice-bath) solution of **2** (0.355 g, 0.5 mmol) in THF (2.5 mL, 0.2 M) phenyl silane (PhSiH₃; 0.092
420 mL, 0.75 mmol) was added followed by tetrakis(triphenylphosphine) palladium (Pd(PPh₃)₄; 0.007 g, 0.00625
421 mmol). The reaction was removed from the cooling bath and stirred for 20 min; *t*_{lc} [PE–DCM 4:1]–EA 30%
422 revealed the reaction was complete. The reaction was concentrated. The crude acid **3** was dried in vacuum
423 and used in the peptide synthesis without purification.

424
425 *Analysis of O- and S-GlcNAc hydrolysis*
426 hOGA- and α -synuclein-derived O- and S-GlcNAc peptides were diluted to 0.5 mM in 50 μ l TBS buffer. To
427 initiate the reaction, CpOGA was added to a final concentration of 0.3 μ M. Hydrolysis reactions were
428 performed at 37 °C for 4 or 24 h. Samples not treated with CpOGA were used as negative controls. To
429 separate the peptides from CpOGA, all samples were passed through a 10 kDa molecular weight cut-off
430 spin column. For MALDI-TOF MS analysis, samples were diluted in 0.1% TFA and 2 pmol was used for
431 loading. 2,5 dihydroxy benzoic acid was used as a matrix. The samples were run in a rapifleX MALDI-TOF
432 MS system.

433
434 *Fluorescence polarization assay*
435 Experiments were performed in black 384-well plates as described previously²³. Reaction mixtures
436 contained (added in order): O- or S-GlcNAc-modified peptide derived from hOGA (VAHS/C(GlcNAc)GA) or
437 α -synuclein (GAVVT/C(GlcNAc)GVTA) at varying concentrations, 16 nM CpOGA^{D298N} inactive mutant and
438 5 nM fluorescent probe (GlcNAcstatin-B-FITC) in TBS buffer pH 7.5 containing 1% DMSO. Fluorescence
439 polarization (in millipolarization units) was measured using a Pherastar FS plate reader at excitation and
440 emission wavelengths of 485 nm and 530 nm, respectively. Background subtraction was performed using
441 reactions that did not contain CpOGA^{D298N} and data were fitted with GraphPad Prism as described

442 previously²³. Assays using O-GlcNAcylated peptides were performed with three technical replicates in three
443 independent experiments. Assays using S-GlcNAcylated peptides were performed with a single technical
444 replicate in three (α -synuclein peptide) or four (hOGA peptide) independent experiments.

445

446 *Crystallography*

447 CpOGA^{D298N} was purified and crystallized as previously described²⁵. Soaking with S-modified peptide was
448 performed by transferring crystals into a 0.5 μ l drop of fresh crystallization buffer containing 10 mM of the
449 peptide for 4 h at 20 °C. The crystals were mounted in nylon loops, cryo-protected in 0.175 M CdSO₄, 0.6 M
450 NaAc buffer containing 20% glycerol and flash-frozen in liquid nitrogen prior to data collection. Diffraction
451 datasets were collected at the ID29 beam line (wavelength 0.9686 Å) of the European Synchrotron
452 Radiation Facility (ESRF, Grenoble, France). Datasets were indexed and integrated with XDS⁴² and further
453 reduced and scaled with Aimless. The CpOGA structure in complex with an S-GlcNAc hOGA peptide was
454 solved by molecular replacement using published CpOGA-(O-GlcNAc hOGA peptide) complex structure
455 (PDB: 2YDQ²⁵) without the ligand as a phase donor in MOLREP⁴³. The resulting model was submitted to
456 several cycles of refinement with REFMAC5⁴⁴ followed by manual modelling with COOT⁴⁵. Statistics of the
457 data collection and model refinement are summarized in Table 1. The Ramachandran statistics are as
458 follows: 96.55% favored, 3.45% additionally allowed. Figures of the structures were generated with Pymol⁴⁶.

459

460 *Cloning*

461 The gene coding for full length TAB1 was cloned as a *Bam*HI-*Not*I fragment into the pCMV-FLAG vector
462 (obtained from DSTT, School of Life Sciences, Dundee, UK) for expression of N-terminal FLAG tag. The
463 products were gel extracted and digested with *Bam*HI and *Not*I restriction enzyme. The products were gel
464 extracted and digested before being ligated into pCMV-FLAG cut with *Bam*HI and *Not*I. The inserts were
465 confirmed by DNA sequencing. Wild type pGEX6P1 TAB1 7-409 construct was produced as described
466 previously²⁸. The S395C mutation was introduced by site-directed mutagenesis based on the QuikChange
467 protocol by Stratagene but using KOD Polymerase. All inserts were confirmed by DNA sequencing. Primers
468 used for cloning and sequencing are listed in Supplementary Table 1.

469

470

471

472 *In vitro* OGT reactions and OGT-CK2 linear fusion

473 *In vitro* OGT reaction (100 μ l) contained 10 μ M TAB1 (7-409 construct), 50 nM full length human OGT in
474 TBS buffer pH 7.5 with 0.1 mg/ml bovine serum albumin (BSA). The reaction was initiated by addition of
475 UDP-GlcNAc to a final concentration of 100 μ M. Reactions were performed at 25 $^{\circ}$ C. After incubation with
476 OGT, the reactions were treated with 3 μ M CpOGA for 2 h at 37 $^{\circ}$ C. 5 μ l of the reaction was taken at
477 different time points, run on the SDS PAGE gel and analyzed by Western blotting using O-GlcNAc TAB1
478 and total TAB1 antibodies. The OGT-CK2 peptide linear fusion was produced as described previously²⁸.

479

480 *Mass spectrometry*

481 TAB1^{S395C} OGT *in vitro* reaction was run on SDS-PAGE, the corresponding TAB1 band was excised and
482 processed by in-gel digestion. The gel slice was washed with water, shrunk with 100 μ l of acetonitrile (ACN)
483 for 5 min at room temperature and reswollen with 50 μ l of 50 mM Tris HCl pH 8.0 twice. Reduction and
484 alkylation were performed in gel using 50 μ l of 5 mM DTT in 50 mM Tris HCl pH 8.0 (shaken for 20 min at
485 65 $^{\circ}$ C) and 50 μ l of 50 mM iodoacetamide in 50 mM Tris HCl pH 8.0 (shaken for 20 min at room
486 temperature). The gel slice was shrunk using 500 μ l ACN for 5 min at room temperature and 50 μ l of 50
487 mM triethylammonium bicarbonate was added to reswell the gel slice. 50-100 μ l of mass spectrometry
488 grade trypsin in 50 mM triethylammonium bicarbonate, containing 5 μ g/ml of trypsin protease (in 50 mM
489 acetic acid) was added and the sample was shaken at 30 $^{\circ}$ C overnight. 100 μ l of ACN was added to
490 completely shrink the gel. The supernatant was transferred to a fresh tube. The gel piece was re-swollen
491 with 50 μ l of 0.1% trifluoroacetic acid (TFA). Digest was extracted twice with 100 μ l of ACN. All extracts
492 were combined, lyophilized in a speed-vac and stored at -20 $^{\circ}$ C. Mass spectrometric analysis was
493 performed by LC-MS/MS on an Orbitrap Fusion tribrid mass spectrometer (Thermo Scientific) coupled to a
494 U3000 RSLC HPLC (Thermo Scientific). Peptides were trapped on a nanoViper Trap column, 2 cm x 100
495 μ m, C18 5 μ m 100 Å (Thermo Scientific, 164564) and then separated on a 50 cm EASY-Spray column
496 (Thermo Scientific, ES803) equilibrated with a flow of 300 nl/min of 3% Solvent B (Solvent A: 2%
497 Acetonitrile, 0.1% formic acid; Solvent B: 80% acetonitrile, 0.08% formic acid). The elution gradient was as
498 follows: time (min): solvent B (%); 0:3, 5:3, 55:25, 74:40, 79:99, 80:3, 90:3. The instrument was operated
499 with the internal mass calibrant (EASY IC) option to improve the mass accuracy of precursor ions and data
500 were acquired in the data-dependent mode. MS1 spectra (m/z 400-1600) were acquired in the Orbitrap

501 with resolution 120,000. The method used was a 'top speed' method. The precursors were isolated using
502 quadrupole with an isolation width of 1.6 Da. The activation type was HCD (Higher-energy Collisional
503 Dissociation) with collision energy at 30% and the fragments were detected in ion trap mass analyzer. The
504 AGC (Automatic Gain Control) target set was 100 and the maximum injection time was set at 250 ms. If an
505 ion in this analysis shows the presence of certain ions, in this case any of HexNAc (204.1), HexNAc
506 fragment (138.1) or HexNAcHex (366.1) then EThcD/Orbitrap analysis of the parent ion was triggered. The
507 ions were isolated using quadrupole and fragmentation method used was ETD (Electron Transfer
508 Dissociation) with HCD supplemental activation (EThcD). The Orbitrap resolution for this step was set at
509 30000. The AGC target was 30000 and the maximum injection time was 150 ms. Data files were analyzed
510 by Proteome Discoverer 2.0 (Thermo Scientific), using Mascot 2.4.1 (www.matrixscience.com), and
511 searching an in-house database containing the relevant sequences. Scaffold
512 (www.ProteomeSoftware.com) was also used to examine the Mascot result files. Allowance was made for
513 the following variable modifications Oxidation (M), HexNAc (S), HexNAc (C). Error tolerances were 10 ppm
514 for MS1, 0.6 Da for HCD MS2 and 20 mmu for EThcD/Orbitrap spectra

515

516 *Cell culture and transfection*

517 IL-1R Hek293 cells²⁷ were grown in DMEM medium supplemented with 10% FBS, 2 mM L-glutamine and
518 1% penicillin/streptomycin (100 U/ml and 100 µg/ml respectively) at 37 °C and 5% CO₂. Hek293 cells were
519 transfected with FLAG-tagged TAB1 using Lipofectamine 3000 reagent (Invitrogen) at a ratio 1:2 (µg:µl)
520 according to manufacturer's instructions. Male mouse embryonic stem cells (AW2 line from MRC Centre for
521 Regenerative Medicine, Institute for Stem Cell Research, University of Edinburgh) were cultured in 0.1%
522 (w/v) gelatin-coated plates in GMEM BHK-21 medium supplemented with 10% fetal bovine serum, 50 µM
523 β-mercaptoethanol, 0.1 mM non-essential amino acids, 1 mM sodium pyruvate and 100 U/ml leukemia
524 inhibitory factor at 37 °C and 5% CO₂. Cell lines tested negative for mycoplasma. GlcNAcstatin G treatment
525 was performed at a final concentration of 1 µM for 24 h. 4Ac5S-GlcNAc treatment was performed at a final
526 concentration of 200 µM for 24 h.

527

528

529

530 *Generation of OGA S405C CRISPR-Cas9 knock-in mouse embryonic stem cells*

531 Paired gRNAs were selected using the website http://www.sanger.ac.uk/htgt/wge/find_crisprs. Annealing
532 oligonucleotides were designed with the appropriate overhangs for cloning into *Bpi*I cut pX335 (Cas9 D10A)
533 and pBABED puro U6. A 3 μ M mix of each annealing oligonucleotide pair were combined in a 100 μ l
534 volume and treated with 1 μ l polynucleotide kinase (Fermentas) in T4 Ligase buffer at 37 °C for 20 min
535 followed by 10 min incubation at 75 °C and finally placed in a heating block at 95 °C. The metal block was
536 removed from the heat source and allowed to cool gradually to room temperature. 1 μ l of a 1/30 dilution of
537 this mixture was added to a ligation reaction containing 20 ng *Bpi*I cut, dephosphorylated destination vector
538 and 1 μ l DNA ligase (Fermentas) in T4 ligase buffer in a 20 μ l final volume. After 25 min at RT a 1 μ l aliquot
539 of the reaction was used to transform DH5-alpha competent cells. Inserts were confirmed by DNA
540 sequencing. A 2 kb PCR product was obtained from 46c mouse genomic DNA and cloned as a *Bam*HI-*Not*I
541 fragment into pGEX6P1. The insert was confirmed to be wild type by DNA sequencing. A 249 bp geneblock
542 containing the desired mutation and silent mutations to eliminate the gRNA recognition sites was ordered
543 from Integrated DNA Technologies. The geneblock was amplified by PCR, the product was gel extracted
544 and introduced into the middle of the 2 kb insert by restrictionless cloning⁴⁷. The changes were confirmed
545 by DNA sequencing.

546 Male mouse embryonic stem cells were co-transfected with pBABED, pX335 and the repair template
547 plasmids using Lipofectamine 3000 (Invitrogen) according to manufacturer's instructions. 24 h post
548 transfection, G-MEM medium (supplemented with 10% fetal bovine serum, β -mercapthoethanol, non-
549 essential amino acids, sodium pyruvate and leukemia inhibitory factor) was substituted with fresh medium
550 containing 1 μ g/ml puromycin. Cells that survived after 24 h of puromycin treatment were dissociated with
551 accutase, and plated onto several 10 cm plates. Colonies were grown for 1-2 weeks and then screened by
552 restriction digestion of a 622 bp PCR product (covering the mutation site) with *Dra*I enzyme. Wild type
553 restriction digestion produced two 231 and 391 bp bands on a 1.3% agarose gel. The S405C mutant
554 produced a single 622 bp band, which was verified by sequencing (Supplementary Fig. 1 and 2). To
555 eliminate the possibility of a false positive due to random integration of the repair template into the genome
556 and to detect the presence of hemizygous genomic deletions, a larger PCR product was obtained. This
557 PCR product encompassed an area outside the repair template and sequencing confirmed the change in
558 the correct location (Supplementary Fig. 3). This confirmed the desired homologous recombination had
559 taken place. Primers used for knock-in generation and sequencing are listed in Supplementary Table 1.

560 In addition to DNA based analysis of mutated cell lines, RNA was extracted from candidate clones
561 containing the S405C mutation. This RNA was subjected to one-step RT-PCR (using Takara Primescript
562 High Fidelity RT-PCR Kit) with primers specific to the next exon outside the area covered by the repair
563 template in both directions. This resulted in a 951 bp PCR product. Sequencing of the resultant product
564 from both ends confirmed the precision of the alteration of the mRNA expressed in these cells
565 (Supplementary Fig. 4). Primers and geneblock sequence are listed in Supplementary Table 1.

566

567 *Western blotting*

568 Cells were scraped in lysis buffer (Cell Signaling Technology, #9803) supplemented with 1 mM PMSF,
569 sonicated and lysates were spun down at 17000 g for 10 min. Supernatants were transferred into fresh
570 tubes and protein concentration was quantified using Bradford assay. Protein samples were prepared using
571 LDS buffer containing 5% β -mercaptoethanol. Samples were run on a 10% SDS PAGE gel. Proteins were
572 then transferred onto nitrocellulose membrane at 100 V for 1 h. Membranes were stained with Ponceau-S
573 to check for successful transfer, washed with 0.2% TBS-Tween and blocked in 5% BSA in 0.2% TBS-
574 Tween. Primary antibodies are listed in Supplementary Table 2. Fluorescence signal from secondary
575 antibodies (Li-Cor) was quantified using Image Studio software and statistical analysis was performed using
576 Prism (GraphPad).

577

578 *O- and S-GlcNAc PEGylation labelling using Gal-T^{Y289L}*

579 The Click-iT™ O-GlcNAc enzymatic labelling system was used according to manufacturer's instructions
580 (Thermo Fisher Scientific) with some modifications. 50-100 μ g of whole cell lysate proteins or 20 μ g of *in*
581 *vitro* GlcNAcylated TAB1 were subjected to Gal-T^{Y289L} labelling. The Gal-T^{Y289L} reaction components were
582 added in the following order to 20 μ l of chloroform/methanol precipitated proteins (in 20 mM HEPES, pH
583 7.9): 24.5 μ l MiliQ water, 40 μ l labelling buffer (component C), 5.5 μ l MnCl₂ (100 mM, component D) and
584 vortexed briefly. 10 μ l 0.5 mM UDP-GalNAz was added, mixed by pipetting and half of the reaction (50 μ l)
585 was removed as an unlabeled negative control. Finally, 4 μ l Gal-TY289L was added to the reaction and
586 mixed by pipetting. Both the reaction and the negative control were incubated at 4 °C overnight.

587 PEGylation of GalNAz-labelled proteins was performed using the Click-iT® Protein Reaction Buffer Kit
588 according to manufacturer's instructions (Thermo Fisher Scientific) with some modifications. MeO-PEG-

589 alkyne (Mw = 5000 Da, IrisBiotech, PEG2830.0500) was prepared beforehand as a 10 mM solution in water
590 and stored at -20 °C. Proteins (20 µl in 1% SDS, 50 mM Tris HCl, pH 8.0) prepared by GalNAz labelling
591 were mixed with 40 µl Click-iT® reaction buffer containing 3.3 mM PEG-alkyne (i.e. 100 µl of PEG-alkyne
592 stock solution was mixed with 200 µl of Click-iT® reaction buffer, component A). 4 µl of CuSO₄ was added,
593 followed by 8 µl of Click-iT® reaction buffer additive 2 solution. The reaction was then incubated at room
594 temperature with 1400 rpm shaking for 1-1.5 h. The samples were prepared in LDS buffer (containing 5%
595 β-mercaptoethanol) and analyzed by Western blotting.

596 *Cycloheximide treatment*

597 mES cells were treated with cycloheximide (Cayman Chemical, dissolved in DMSO) at a final concentration
598 of 20 µg/ml for different time points before lysis. DMSO treatment was used as a negative control.

599

600 *OGA thermal stability assay in cell lysates*

601 mES cells were lysed as described above and subjected to a range of temperatures in a thermomixer. After
602 5 min of incubation at each temperature, the lysates were centrifuged and soluble fraction was removed for
603 subsequent Western blot analysis.

604

605 **Reporting Summary**

606 Further information on experimental design is available in the Nature Research Reporting Summary linked
607 to this article.

608

609 **Data Availability**

610 Atomic coordinates and structure factors for the CpOGA-(S-GlcNAc peptide) complex structure are
611 deposited in the Protein Data Bank under the accession code PDB 6RHE. Source data for Fig. 1c, 2c, 3a,
612 3b, 3c and Extended Data Fig. 1b, 6, 7 are available with the paper online. All other data are available upon
613 reasonable request to the corresponding author.

614 **Methods-only references**

- 615 40. Rafie, K., Gorelik, A., Trapannone, R., Borodkin, V. S. & Aalten, D. M. F. Thio-linked UDP-peptide
616 conjugates as O-GlcNAc transferase inhibitors. *Bioconjugate Chemistry* (2018). doi:
617 10.1021/acs.bioconjchem.8b00194
- 618 41. Zhu, X., Pachamuthu, K. & Schmidt, R. R. Synthesis of S-linked glycopeptides in aqueous solution.
619 *J. Org. Chem.* (2003). doi: 10.1021/jo034148n
- 620 42. Kabsch, W. XDS. *Acta Crystallogr. Sect. D Biol. Crystallogr.* **66**, 125–132 (2010). doi:
621 10.1107/S0907444909047337
- 622 43. Vagin, A., Teplyakov, A. & IUCr. Molecular replacement with *MOLREP*. *Acta Crystallogr. Sect. D*
623 *Biol. Crystallogr.* **66**, 22–25 (2010). doi: 10.1107/S0907444909042589
- 624 44. Murshudov, G. N., Vagin, A. A. & Dodson, E. J. Refinement of macromolecular structures by the
625 maximum-likelihood method. *Acta Crystallogr. Sect. D-Biological Crystallogr.* **53**, 240–255
626 (1997). doi: 10.1107/S0907444996012255
- 627 45. Emsley, P. & Cowtan, K. Coot: model-building tools for molecular graphics. *Acta Crystallogr D Biol*
628 *Crystallogr* **60**, 2126–2132 (2004). doi: 10.1107/S0907444904019158
- 629 46. Delano, W. L. & Bromberg, S. *PyMOL User's Guide*. DeLano Scientific LLC (2004).
- 630 47. Van Den Ent, F. & Löwe, J. RF cloning: A restriction-free method for inserting target genes into
631 plasmids. *J. Biochem. Biophys. Methods* (2006). doi: 10.1016/j.jbbm.2005.12.008

